

# Influence of Conformation on Conductance of Biphenyl-Dithiol Single-Molecule Contacts

Artem Mishchenko,<sup>†</sup> David Vonlanthen,<sup>‡</sup> Velimir Meded,<sup>§</sup> Marius Bürkle,<sup>||</sup> Chen Li,<sup>†</sup> Ilya V. Pobelov,<sup>†</sup> Alexei Bagrets,<sup>§</sup> Janne K. Viljas,<sup>||</sup> Fabian Pauly,<sup>\*,||</sup> Ferdinand Evers,<sup>\*,§,⊥</sup> Marcel Mayor,<sup>\*,†,§</sup> and Thomas Wandlowski<sup>\*,†</sup>

<sup>†</sup>Department of Chemistry and Biochemistry, University of Bern, 3012 Bern, Switzerland, <sup>‡</sup>Department of Chemistry, University of Basel, 4003 Basel, Switzerland, <sup>§</sup>Institute of Nanotechnology, Karlsruhe Institute of Technology, P.O. Box 3640, 76021 Karlsruhe, Germany, <sup>||</sup>Institut für Theoretische Festkörperphysik, <sup>⊥</sup>Institut für Theorie der Kondensierten Materie, and University of Karlsruhe, 76128 Karlsruhe, Germany

**ABSTRACT** The conductance of a family of biphenyl-dithiol derivatives with conformationally fixed torsion angle was measured using the scanning tunneling microscopy (STM)-break-junction method. We found that it depends on the torsion angle  $\varphi$  between two phenyl rings; twisting the biphenyl system from flat ( $\varphi = 0^\circ$ ) to perpendicular ( $\varphi = 90^\circ$ ) decreased the conductance by a factor of 30. Detailed calculations of transport based on density functional theory and a two level model (TLM) support the experimentally obtained  $\cos^2 \varphi$  correlation between the junction conductance  $G$  and the torsion angle  $\varphi$ . The TLM describes the pair of hybridizing highest occupied molecular orbital (HOMO) states on the phenyl rings and illustrates that the  $\pi$ - $\pi$  coupling dominates the transport under “off-resonance” conditions where the HOMO levels are well separated from the Fermi energy.

Understanding of the charge transport characteristics of molecules in nanoscale metal–molecule–metal junctions is of fundamental interest and represents a key step toward the realization of molecule-based electronics.<sup>1,2</sup> Several experimental approaches have been employed to measure transport through single and small groups of molecules. Examples are mechanical<sup>3–6</sup> or electromigration<sup>7,8</sup> break junctions, nanopores,<sup>9</sup> crossed-wire junctions,<sup>10</sup> mercury drop electrodes,<sup>11</sup> and a variety of scanning probe methods based on either scanning tunneling spectroscopy (STS)<sup>12–18</sup> or conducting probe atomic force microscopy (CP-AFM).<sup>19,20</sup> These measurements differ in the following criteria: (i) formation of reproducible contacts between molecules and two probing electrodes, (ii) access of “signatures” of single molecules, and (iii) algorithm of data analysis.

These experimental results and numerous contributions on theoretical aspects of charge transport through molecular junctions<sup>1,21</sup> suggest that the transport characteristics are controlled by the intrinsic properties of the molecules, the contacts (“alligator clips”), and the metal leads. These include the molecular length, conformation, the gap between HOMO and LUMO, the alignment of this gap to the metal Fermi level, and the metal–molecule coordination geometry. Other factors of influence comprise temperature, mechanical stress, environment (UHV, gas, or solution phase), and the applied potential. Understanding of relationships between molecular structure and electronic transport characteristics of single-molecule junctions is a major challenge. Progress may lead

to the rational design of functional molecules as active components in future electronic circuits. To date, the properties of a specific molecular configuration and binding geometry with respect to stability and transmittivity have not been observed directly. Most experimental strategies are instead based on statistical ensemble measurements of individual junctions.<sup>5,6,14–17,19</sup> An important step to bridge our understanding between ensemble and single-junction characteristics represents the concept of “molecular families”.<sup>22</sup> The ideal strategy is based on the systematic variation of one structure element of the junction, such as length,<sup>14,17,19,23,24</sup> anchoring group,<sup>25</sup> electronic structure,<sup>26,27</sup> or molecular conformation.<sup>16,17,22,28</sup> In combination with carefully designed transport experiments on the single-molecule level corresponding changes in physical observables are analyzed.

The present study aims at exploring experimentally and theoretically the correlation between torsion angle  $\varphi$  and conductance in a series of single-molecule BPDT junctions as formed between two gold electrodes. Chemical tuning by incorporation of an alkyl chain of variable length in 2,2'-position (“molecular strap”) controls the torsion angle between the two interconnected aromatic rings, guaranteeing minimum motion and conformational freedom of the bridge without changing the electronic character of the substituents and the length of the bridging molecule. For instance, the distance between the two –SH anchoring groups remains rather constant and amounts to  $\sim 1.06$  nm. The choice of the thiol anchoring groups ensures a strong chemical bonding to the leads with the current flow mainly modulated by the molecular HOMO level.<sup>29</sup>  $\pi$ - $\pi$  coupling dominates electron transport in aromatic bridges and transport can be manipulated and tailored by controlling the degree of elec-

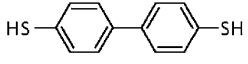
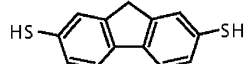
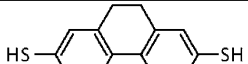
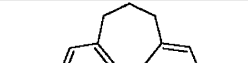
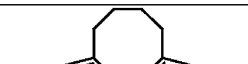
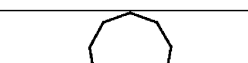
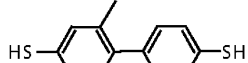
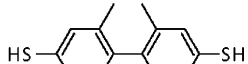
\* To whom correspondence should be addressed. E-mail: (F.P.) fabian.pauly@kit.edu; (F.E.) ferdinand.evers@int.fzk.de; (M.M.) marcel.mayor@unibas.ch; (T.W.) thomas.wandlowski@dcb.unibe.ch.

Received for review: 09/17/2009

Published on Web: 12/21/2009



TABLE 1. Experimental (Columns 3,4) and Theoretical (Columns 3,5,6) Results for the Torsion Angle and the Conductance<sup>a</sup>

molecule	structure	Torsion angle $\varphi$		$G/G_0$ ( $\varphi$ ) DFT atop-atop	$G/G_0$ ( $\varphi$ ) DFT bridge-bridge
		x-ray (DFT SH- terminated)	$G/G_0$ experiment		
<b>M1</b>		36.4 <sup>o29</sup> (44.9 <sup>o</sup> )	1.7·10 <sup>-4</sup> ± 2·10 <sup>-5</sup>	5.0·10 <sup>-2</sup> (34.2 <sup>o</sup> )	1.3·10 <sup>-1</sup> (12.9 <sup>o</sup> )
<b>M2</b>		1.1 <sup>o</sup> (2.4 <sup>o</sup> )	1.4·10 <sup>-4</sup> ± 8·10 <sup>-6</sup>	9.9·10 <sup>-2</sup> (2 <sup>o</sup> )	1.4·10 <sup>-1</sup> (0.1 <sup>o</sup> )
<b>M3</b>		16.8 <sup>o</sup> (20.3 <sup>o</sup> )	2.2·10 <sup>-4</sup> ± 2·10 <sup>-5</sup>	8.9·10 <sup>-2</sup> (18.9 <sup>o</sup> )	1.2·10 <sup>-1</sup> (19.3 <sup>o</sup> )
<b>M4</b>		44.7 <sup>o</sup> (46.7 <sup>o</sup> )	1.3·10 <sup>-4</sup> ± 2·10 <sup>-5</sup>	4.6·10 <sup>-2</sup> (46.4 <sup>o</sup> )	7.4·10 <sup>-2</sup> (42.1 <sup>o</sup> )
<b>M5</b>		57.8 <sup>o</sup> (61.3 <sup>o</sup> )	7·10 <sup>-5</sup> ± 2·10 <sup>-5</sup>	1.8·10 <sup>-2</sup> (61.1 <sup>o</sup> )	3.8·10 <sup>-2</sup> (53.0 <sup>o</sup> )
<b>M6</b>		71.5 <sup>o</sup> (70.5 <sup>o</sup> )	1.7·10 <sup>-5</sup> ± 3·10 <sup>-6</sup>	8.2·10 <sup>-3</sup> (72.0 <sup>o</sup> )	1.6·10 <sup>-2</sup> (62.5 <sup>o</sup> )
<b>M7</b>		79.7 <sup>o</sup> (89.7 <sup>o</sup> )	1.3·10 <sup>-5</sup> ± 2·10 <sup>-6</sup>	8.4·10 <sup>-4</sup> (86.9 <sup>o</sup> )	4.1·10 <sup>-2</sup> (50.0 <sup>o</sup> )
<b>M8</b>		89.0 <sup>o</sup> (89.6 <sup>o</sup> )	9.0·10 <sup>-6</sup> ± 2·10 <sup>-6</sup>	4.7·10 <sup>-4</sup> (88.6 <sup>o</sup> )	5.0·10 <sup>-4</sup> (96.0 <sup>o</sup> )

<sup>a</sup> The mean value of the conductances and the corresponding standard deviations (error bars in Figure 3A) were obtained from averaging the peak positions of the conductance histograms as recorded for different bias voltages as well as from additional experiments at the same bias voltage. The deviations between atop-atop and bridge-bridge geometry occur because the molecular conformation for the bridge-bridge geometry (column 6) has been optimized subject to a geometrical constraint set by the gold electrodes (see Figure 4 and Supporting Information, section D).

tron delocalization. Examples are the triplet energy transfer in a series of mixed Ru-Os-bis(2,2':6',2'') terpyridine complexes attached to biphenyl spacer groups,<sup>50</sup> the electron transfer characteristics of ferrocene covalently bound to OPE rods,<sup>31</sup> the conductance of 4,4'-bipyridine,<sup>32,33</sup> or oligoaniline<sup>34</sup> junctions. The effect of rotating the middle ring of 1,4-bis-phenylethynyl-benzene on the conductance was estimated by Sankey et al. using the Landauer formalism in combination with a complex band structure analysis.<sup>35</sup> Venkataraman et al. showed in a series of terminally amine-functionalized biphenyls comprising electron-donating and withdrawing substituents that the conduction scales approximately linearly with  $\cos^2 \varphi$ .<sup>16</sup> However, the role of

geometric and electronic effects of the substituents is still being actively discussed.<sup>16,22,26,28,29,36</sup> The present paper aims at addressing this issue experimentally and theoretically.

**Experiment.** To show that the  $\cos^2 \varphi$  law is universal, we measured the conductance  $G$  of thiol-terminated biphenyl derivatives with systematically varied torsion angle between the two phenyl rings, using a STM-break-junction technique.<sup>17</sup> The molecules studied (Table 1) were synthesized as acetyl-protected derivatives (for details of the synthesis and characterization we refer to refs 37 and 38) and were deprotected in situ during the transport experiments. We emphasize that we avoided using strongly electron-donating or electron-withdrawing side groups to control the molecular

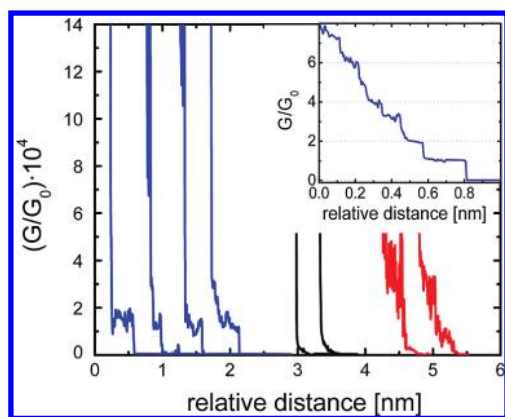


FIGURE 1. Examples of the three types of conductance–distance (retraction) traces for **M1** at  $V_{\text{bias}} = 0.1$  V: type I (black), smooth exponentially decaying or sharp abrupt curves; type II (red), non-monotonous, noisy curves; and type III (blue), curves with pronounced steps. The inset shows a typical trace for the breaking of gold nanocontacts in the presence of **M1** in a larger conductance range.

conformation. The introduced alkyl bridges are known to act as band insulators.<sup>17</sup> Therefore, no parasitic additional transport channels are created.

Conductances of molecular junctions Au–BPDT–Au were measured by the repeated formation and breaking of atomic contacts between a gold STM tip and a Au(111) sample in 0.25 mM solutions of the respective biphenyl derivatives in a mixture of THF and mesitylene (1:4, v/v). For details on the experimental setup and measuring procedures we refer to our previous publications 17 and 39 as well as to the Supporting Information, section A.

Figure 1 illustrates selected conductance–distance traces (increasing tip–sample distance) in the presence of 0.25 mM biphenyl-4,4'-dithiol (**M1**). As visible from the inset, characteristic quantized conductance steps occur at integer multiples of  $G_0 = 2e^2/h$ , which we attribute to the breaking of previously formed gold–gold atomic contacts. Additional features develop at  $G < 10^{-3}G_0$ . We observe three types of curves, (i) type I curves (60%) are exponential and represent direct electron tunneling between gold tip and substrate without molecular junctions being formed, (ii) type II curves (10–20%) are nonmonotonous with large fluctuations, which we attribute to mechanical instabilities<sup>17</sup> or switching between single and multimolecular junctions,<sup>40</sup> (iii) type III curves (20–30%) are nonexponential, and exhibit well-defined steps separated by characteristic plateaus of 0.05–0.30 nm length. These plateaus occur within a narrow distribution of conductance values and are not observed in control experiments in the absence of molecules in solution. They are assigned to the breaking of individual molecular junctions bridging the gap between the two gold leads. The plateaus are somewhat noisy, which is related to changes in molecular geometry and molecule–electrode bonding, mechanical stress, or electronic noise upon pulling the junction.<sup>17</sup> Repeated measurements lead to the statistical determination of the junction properties. The peaks in the

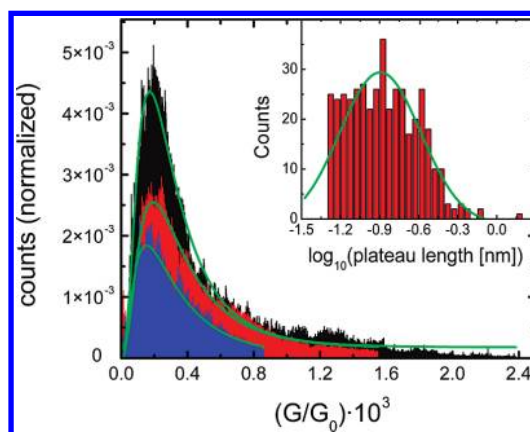


FIGURE 2. Plateau-point histograms for **M1**: (black)  $V_{\text{bias}} = 0.065$  V, (red)  $V_{\text{bias}} = 0.1$  V, and (blue)  $V_{\text{bias}} = 0.18$  V. The inset shows a typical plateau length histogram constructed based on traces with  $V_{\text{bias}} = 0.1$  V.

low-bias conductance histograms correspond to the most probable conductance of a specific molecular junction, and the width of the peaks reflects the microscopic variations from junction to junction. We notice that the algorithm of data analysis was designed such that traces of types I and II did not contribute to the construction of the conductance histogram. For details we refer to the Supporting Information, sections B and C.

Figure 2 shows, as an example, the plateau data-point histogram of 0.25 mM biphenyl-4,4'-dithiol (**M1**) at three bias voltages in a linear representation. Each histogram, constructed of about 1000 individual (type III) traces out of 3000 totally recorded, reveals a distinct maximum. Additional well-separated conductance peaks were not observed. Control experiments with bare THF/mesitylene, e.g. in the absence of **M1**, did not show this feature, indicating clearly a **M1**-related junction response in Figure 2. The position of the peak, which is taken as the most probable single junction conductance  $G = (1.7 \pm 0.2) \times 10^{-4}G_0$  (Table 1), was estimated by fitting a log-normal distribution to the experimental data. The peak position from individual experiments within the low bias regime ( $|V_{\text{bias}}| < 0.30$  V) is well reproducible. The broad asymmetric tail region toward higher conductance values could be related to junctions with multiple molecules, modifications in substrate–adsorbate coordination or atomic rearrangements upon stretching,<sup>17,41,42</sup> local surface roughness,<sup>28</sup> or changes of the torsion angle of **M1** due to the low energy barrier of about 0.1 eV for ring rotation of the unsubstituted biphenyl unit.<sup>43</sup> We emphasize that the measurement time of a single conductance–distance trace (ca. 50 ms) is long compared to the time scale for molecular rotations in solution (ps),<sup>44</sup> so that the conductance level of each step in a single trace is the thermal average over many dynamic fluctuations. We also notice that the analysis of the stretching distance for **M1** leads to the most probable value of  $0.13 \pm 0.05$  nm (inset to Figure 2). A small number of junctions can even be stretched up to 0.40 nm. No obvious correlation is found between stretching distance and junc-

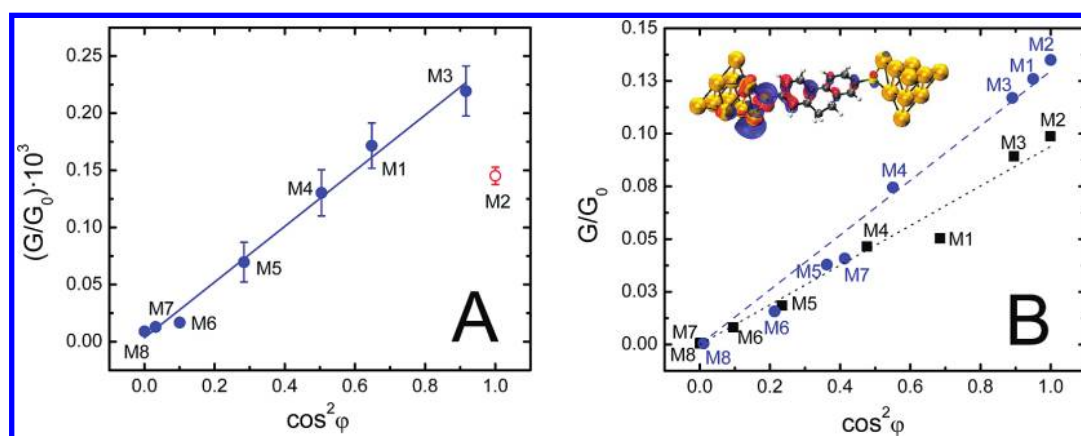


FIGURE 3. (A) Experimentally determined conductance of thiol-terminated biphenyl molecules vs  $\cos^2 \varphi$ , where  $\varphi$  is the torsion angle of the molecules as given by the X-ray data in Table 1. The solid line is the linear fit to all molecules studied, M2 excluded. (B) Conductance obtained from DFT-based transport calculations as a function of  $\cos^2 \varphi$ : (squares) atrop-atop and (circles) bridge-bridge bonding. Dotted and dashed lines represent linear fits  $G = a_{\text{DFT}} \cdot \cos^2 \varphi$  with slopes  $a_{\text{DFT}} = 0.094G_0$  (atop-atop) and  $a_{\text{DFT}} = 0.130G_0$  (bridge-bridge). Variations of  $\varphi$  for the molecules (e.g., M1, M7) arise from different geometric constraints imposed when constructing the contacts. Inset upper left: Dominant transport channel for M3, demonstrating the importance of the  $\pi$ -states for conduction.<sup>45</sup>

tion conductance. This observation together with the narrow distribution of the step-average conductance leads to the conclusion that the spread in the conductance originates primarily from variations in the conductance across different junctions rather than variations in conductance during junction elongation before breaking.<sup>41</sup>

Introducing a bridging alkyl chain  $(-\text{CH}_2)_n$ ,  $n = 1-5$ , in the 2,2'-position (M2 to M6) or  $-\text{CH}_3$  substitution in 2,2' (M7) and 6,6' position (M8) hinders the free rotation and enables tuning the torsion angle between the two phenyl rings from  $\varphi = 0$  to  $90^\circ$ . The values of  $\varphi$  were estimated experimentally by an X-ray structure analysis of acetyl-protected derivatives<sup>38</sup> and theoretically via density functional theory (DFT) calculations (Table 1, column 3). As the angle between the two phenyl rings increases, the conductance drops from  $2.2 \times 10^{-4}G_0$  (M2) to  $9.0 \times 10^{-6}G_0$  (M8), i.e. by a factor of about 25. The lowest conductance was found for 2,2',6,6'-tetramethyl-biphenyl-4,4'-dithiol (M8) with  $\varphi = 89^\circ$ .

Figure 3A displays a linear correlation between the experimentally obtained conductance of the BPDT derivatives and  $\cos^2 \varphi$ . The fluorene derivative M2 appears to be an exception. Using  $G = b + a \cos^2 \varphi$  and excluding M2 from the data fit, we estimate the slope and the intersection as  $a_{\text{ex}} = (2.44 \pm 0.097) \times 10^{-4}G_0$  and  $b_{\text{ex}} = (3.4 \pm 4.7) \times 10^{-6}G_0$ , respectively. The residual conductance  $b_{\text{ex}}$  at  $\varphi = 90^\circ$  stems mostly from  $\sigma$ - $\pi$  couplings.<sup>35,46</sup> The much higher value of the slope  $a_{\text{ex}}$  suggests that the  $\pi$ - $\pi$  overlap between the phenyl rings dominates the junction conductance.<sup>16,29,36,47</sup>

**Theory.** The experimental observations are fully consistent with expectations based on DFT calculations for the biphenyl derivatives M1-M8 coupled to gold electrodes and estimates based on a simple two-level model (TLM) of molecular transport. For the former we have used the quantum chemistry package TURBOMOLE<sup>48,49</sup> with the BP86 functional<sup>50,51</sup> and basis sets of double- $\zeta$  quality

(triple- $\zeta$  for geometry relaxations), including polarization functions.<sup>52,53</sup> Transport calculations are based on the Landauer formalism as implemented in homemade simulation packages.<sup>54,55</sup> For further technical details we refer to the Supporting Information, sections D and E.

**Junction Structure.** Our electronic structure calculations reveal that the torsion angle  $\varphi$  of the isolated biphenyl derivatives in the ground state depends only slightly on terminations, such as  $-\text{H}$ ,  $-\text{SH}$  or  $-\text{S}-\text{Au}_1$  (i.e., attached to a single gold atom). The agreement of the angles with those of the experimentally determined solid-state structure at room temperature is encouraging (Table 1 and Supporting Information, Table S1). In the next step, we represent the molecular junction as an "extended molecule" composed of the various BPDT derivatives M1 to M8 bridging two pyramids of 14 to 120 gold atoms (Figure 4 and Figure S9, Supporting Information). The experimental lattice constant of 0.408 nm was fixed for the bulk part of the gold fcc pyramids, while relaxed configurations were found for the BPDT molecules coupled to few gold atoms assuming different gold-sulfur coordination geometries. Specifically, we treated the atrop-atop and the bridge-bridge configurations, where the sulfur is bonded to one or two atoms of the gold pyramids. Hollow sites and sulfur coordinated to gold adatoms were not considered systematically, because according to recent experimental<sup>17,56</sup> and theoretical reports<sup>35,57</sup> they are probably not representative of the sulfur-gold surface coordination geometry.

The torsion angle  $\varphi$  for the  $-\text{S}-\text{Au}_1$  terminated isolated molecules is close to the crystallographic measurements and by construction identical to those of the "extended molecules" in the atrop-atop coordination (Table 1). However, the corresponding results for  $\varphi$  for the bridge-bridge conformations show some deviations (Table 1). They result from the geometric constraint imposed during the geometry optimization of the extended cluster that primitive vectors

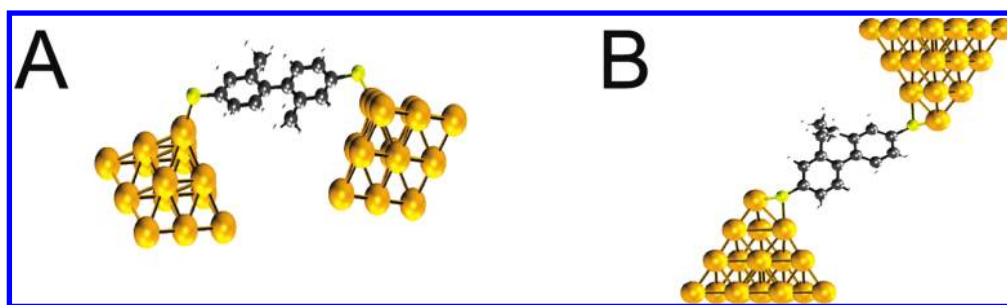


FIGURE 4. Examples of junction geometries: (A) M7 attached to gold pyramids in atop-bonded and (B) M4 attached in bridge-bonded position. Relaxation of the molecule in the latter case has been subject to the constraint that the primitive vectors of the Bravais lattice of the two pyramids are the same.

of the two gold electrodes are identical. The results indicate that the alkyl chains stabilize the torsion angle most effectively for short chains (see  $\varphi$  for **M5** and **M6**). Moreover, particularly pronounced variations for **M1** and **M7** reflect the small steric repulsion of the hydrogens in ortho positions and the resulting low energy barrier for phenyl-ring rotation.<sup>29,43</sup> Further aspects regarding geometric structure optimization are detailed in the Supporting Information, section D.

**Transport.** The conductances of **M1–M8** obtained from the combination of DFT and Landauer theory for the two different bonding geometries are compiled in Table 1, columns 5 and 6, and are displayed in Figure 3B. The fits of  $G = a_{\text{DFT}} \cdot \cos^2 \varphi$  to both series of data reveal a nearly linear behavior, in agreement with the measurements (Figure 3A). On the other hand, we notice that the slopes  $a_{\text{DFT}} = 0.094G_0$  (atop) and  $a_{\text{DFT}} = 0.13G_0$  (bridge) are approximately 3 orders of magnitude higher as compared to the experimental value  $a_{\text{ex}} = 2.44 \times 10^{-4}G_0$  (see discussion below for further details). We have neglected in our fits the residual conductance  $b_{\text{DFT}}$  at  $\varphi = 90^\circ$ . It is given approximately by the conductance of **M8** and is, similar to the experiments, 2 orders of magnitude smaller than  $a_{\text{DFT}}$ .

The main result of the transport measurements and theory is easily understood in terms of a two-level model (TLM). The electron path through the “extended molecule” (Figure 4) can be described by three barriers. Two of them represent the coupling to the leads and the third one is defined by the torsion angle  $\varphi$  between the phenyl rings. These barriers are quite high, as is already suggested from the fact that the experimental conductance is much smaller than  $G_0$ . From previous investigations<sup>46,58,59</sup> of the transport through benzene–dithiol (BDT), it is clear that one deals with hole transport; only the HOMO states of each benzene ring can be involved, since the LUMOs are further away in energy by several eV.

Therefore, the transmission can be described with the TLM using three parameters only, namely  $\varepsilon_0$ ,  $V(\varphi)$ , and  $\Gamma$ . Here,  $\varepsilon_0$  describes two energy levels, which are doubly degenerate for  $\varphi = 90^\circ$ , and correspond to wave functions localized on the left and right phenyl ring [ $\varepsilon_{a,s}(\varphi) = \varepsilon_0 \pm V(\varphi)$ ]. The hopping amplitude  $V(\varphi)$  to transfer electrons from one phenyl ring to another is essentially an overlap matrix

element of the two  $\pi$  systems of the adjacent phenyl rings.  $V(\varphi)$  is controlled by the torsion angle  $\varphi$  and will be represented by  $V_1 \cos \varphi$  where we ignore residual  $\sigma$ – $\pi$  couplings.  $\Gamma$  quantifies the lifetime broadening, that is, the coupling of the molecular HOMO levels to the leads, which considers the contact configuration. The transmission function  $T(E)$  is then given by

$$T(E) = \left| \frac{\Gamma V(\varphi)}{(E - \varepsilon_a(\varphi) - i\Gamma/2)(E - \varepsilon_s(\varphi) - i\Gamma/2)} \right|^2 \quad (1)$$

The conductance in units of  $G_0$  is given by the transmission  $G = T(E_F)$  evaluated at the Fermi level  $E_F$ .

The model predicts in the off-resonant situation, for example, for  $|E_F - \varepsilon_0| \gg \Gamma, V$ , that the conductance is linear in  $\cos^2 \varphi$ :  $G \approx a_{\text{TLM}} \cdot \cos^2 \varphi$  with  $a_{\text{TLM}} = [\Gamma V_1 / (E_F - \varepsilon_0)^2 + \Gamma^2/4]^2$ . The slope  $a_{\text{TLM}} = T_\Gamma \cdot T_{V1}$  is the product of two factors with  $T_\Gamma = \Gamma^2 / [(E_F - \varepsilon_0)^2 + \Gamma^2/4]$  representing the transmission through a single ring and  $T_{V1} = V_1^2 / [(E_F - \varepsilon_0)^2 + \Gamma^2/4]$  the biphenyl-internal transmission from ring to ring. Because of the off-resonant condition, one expects that  $T_\Gamma$  should be quantitatively close to the conductance of BDT,  $G_{\text{BDT}}$ . A second important insight concerns the prefactor  $c_2$  of the leading corrections  $\cos^4 \varphi$ . The TLM predicts that  $c_2 = 2a_{\text{TLM}} T_{V1} (1 - \gamma^2) / (1 + \gamma^2)$ , where  $\gamma = \Gamma/2(E_F - \varepsilon_0)$ . The interesting information comes with the factor  $(1 - \gamma^2)$ , which indicates that due to cancellations  $c_2$  may remain quite small if  $\gamma \approx 1$  even though  $T_{V1}$  is already of order unity.

To obtain the model parameters  $\varepsilon_0$ ,  $V_1$ , and  $\Gamma$  for each molecular junction, we fitted  $T(E)$  (eq 1) to the transmission functions calculated with the DFT-based Landauer formalism.<sup>54,55</sup> Figure 5A shows the splitting between the symmetric and the antisymmetric orbitals  $\varepsilon_s$  and  $\varepsilon_a$  with respect to  $E_F$  as a function of  $\varphi$ . Only a slight curvature is seen with a trend to lower energies, which indicates a weak dependence  $\varepsilon_0(\varphi)$ . For the degenerate case  $\varphi = 90^\circ$ , we obtain  $\varepsilon_0 - E_F \approx -0.9$  eV (atop–atop) and  $\varepsilon_0 - E_F \approx -1.3$  eV (bridge–bridge). The data plotted in Figure 5B also confirms that the level splitting,  $2V(\varphi)$ , is indeed almost linear with  $V(\varphi) = V_1 \cos \varphi$  and  $V_1 = 0.55 \pm 0.05$  eV for atop–atop and a considerably higher value,  $V_1 = 0.81 \pm 0.07$  eV, for bridge–bridge coordination. We also find that the third model parameter,  $\Gamma$ , has a

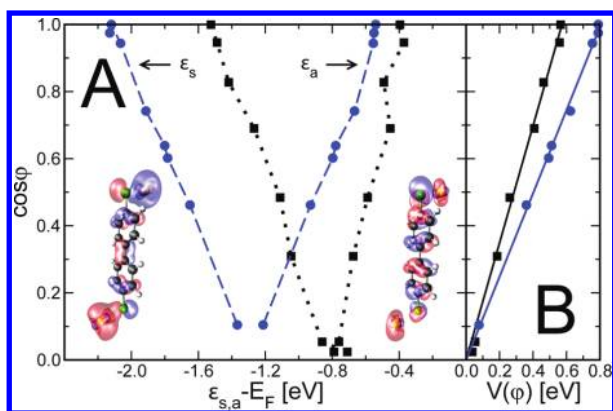


FIGURE 5. (A) The HOMO doublet with its symmetric (left) and antisymmetric (right) orbitals, and the energies  $\epsilon_{s,a}$  as a function of the torsion angle between the two phenyl rings. Results are for the atop-atop geometry (black, squares) and the bridge-bridge geometry (blue, circles). (B) Growth of the effective inter-ring coupling  $V(\varphi) = |\epsilon_a - \epsilon_s|/2$ . Solid lines are linear fits  $V(\varphi) = V_1 \cos \varphi$  with  $V_1 = 0.55$  eV (atop-atop) and  $V_1 = 0.81$  eV (bridge-bridge). The linear behavior is characteristic of the  $\pi$ - $\pi$  coupling.

negligible variation with  $\varphi$ , which could be expected following the logic of the TLM. Specifically,  $\Gamma = 0.37 \pm 0.02$  eV (atop-atop) and  $\Gamma = 0.6 \pm 0.04$  eV (bridge-bridge) were estimated for the two coordination geometries. See also Supporting Information, section E for further details.

**Discussion.** Our theoretical analysis clearly confirms the naive expectation that the angular dependence of the overlap of the  $\pi$ -orbitals plays the dominant role for electronic transport in the range of torsion angles  $0 \leq \varphi \leq 80^\circ$ . Moreover, theory also suggests that the dependence of the conductance on  $\cos^2 \varphi$  is linear for all  $\varphi$ . A linear dependence is also seen in experiments, when assuming that the torsion angle in the junctions is close to its crystalline equilibrium value. Thus, it is suggested that the statistical fluctuations about the (relaxed) equilibrium value of the torsion angle of the molecule may be relatively small even inside the molecular junction.

We notice that the absolute values of the theoretically (DFT) determined conductances are 3 orders of magnitude higher than in the experiments. This may be attributed to an insufficient accuracy in the level alignments<sup>60</sup> and level broadenings.<sup>61</sup> Moreover, as already suggested from the broad distributions in the experimental conductance histograms (Figure 2 and Supporting Information, section C), many experimental factors, which are not understood in full detail and therefore cannot be accounted for in the theoretical modeling, may further diminish the precise values of “typical and average” conductances. Examples are the exact coordination geometry upon stretching, the molecular tilt and/or the atomic structure of the electrode at the moment of bond breaking (cf. discussion in refs 28 and 62). Moreover, if docking to hollow sites of electrodes should be realized in our experiments after all, then our preliminary calculations suggest that these bonding geometries would contribute to the statistical average with conductances an

order of magnitude below those of bridge-bridge and atop-atop configurations.

In addition, it is conceivable that transport under experimental conditions is not fully coherent, opposite to what was the basic assumption underlying our transport calculations. We emphasize that our essential statements remain valid, however, even in the strongly incoherent limit, where the molecular resistance,  $R = G^{-1}$ , is the sum of the two independent contributions,  $R = R_\Gamma + R_\varphi$ . Again, the first term roughly relates to the resistance of BDT,  $R_\Gamma \approx R_{\text{BDT}}$ , while the second one describes inter-ring transport,  $R_\varphi = 1/T_1^{\text{incoh}} \cos^2 \varphi$ .

So far we discussed the origin of the general trends exhibited in the conductance traces. Molecule-specific deviations, such as binding geometry, or changes in the torsion angle upon surface coordination, which are accessible in our calculations, are not resolved within the experiment mainly because the binding geometry are not sufficiently well controlled. We also mention that a particular experimental feature, namely the surprisingly low conductance of the fluorene derivative **M2**, is not reproduced in our calculations.

Finally, we compare our results with those found in the literature. The TLM leads to a conservative estimation of  $T_{V_1} \approx 0.25 \pm 0.10$ , which represents the internal transmission across the biphenyl unit. With the experimental slope  $a_{\text{ex}} = 2.44 \times 10^{-4} G_0$  we estimate  $T_\Gamma \sim 10^{-3}$ . The value of  $T_\Gamma$  should be close to  $G_{\text{BDT}}$ . Unfortunately, the experimental data for  $G_{\text{BDT}}$  varies over more than 2 orders of magnitude and thus the comparison is difficult. Examples are  $0.011 G_0$ ,<sup>63</sup>  $5.8 \times 10^{-4} G_0$ ,<sup>3</sup>  $1.1 \times 10^{-4} G_0$ ,<sup>28</sup> or  $5 \times 10^{-5} G_0$ .<sup>64</sup>

A comparison of our work with the study of Venkataraman et al.<sup>16,22,60</sup> on a related family of molecules with amino linker groups is more encouraging. These authors estimated the experimental slope  $a_{\text{ex}}(\text{NH}_2) \approx 1.5 \times 10^{-3} G_0$ . With  $T_{V_1} \approx 0.25$  we obtain for the junction conductance of biphenyl-diamine (BDA)  $G_{\text{BDA}} \approx 6 \times 10^{-3} G_0$ . This value is in good agreement with data reported in ref 16 but deviates considerably from measurements published by Haiss et al. employing the so-called  $i(t)$  method ( $G_{\text{BDA}} \approx 1.1 \times 10^{-4} G_0$ ).<sup>28</sup> The variations in conductance of the diamines might be related to an uncontrolled but different substrate surface morphology<sup>62</sup> and adsorbate coordination<sup>17</sup> and/or other technical details of the chosen experimental protocols. The distinctly larger variation of conductance data for aromatic dithiols as compared to the family of diamines might reflect the less uniform or less well-defined adsorption geometry of the former<sup>17,28,56,57</sup> as compared to the latter.<sup>16,22,24,60</sup> Investigations along these lines are in progress in our groups.

**Conclusions.** We have studied a family of BPDT molecules with gradually varied torsion angles between the two phenyl units, tuned chemically by introducing  $-\text{CH}_3$  substituents or a  $-(\text{CH}_2)_n-$  bridge with  $n$  ranging between 1 and 5. The junction conductance increases linearly with  $\cos^2 \varphi$ , as reported previously with amino-linkers, and covers almost the full angular range. Our study provides a clear example

of the reproducible measurement of a molecule-specific property, the pronounced  $\cos^2 \varphi$  variation. A two level model motivated and parametrized by extensive DFT-based transport calculations corroborates this further. We demonstrated that the transmission factorizes in an “off-resonance” junction, such that “ring-to-ring” and “electrode-ring” transmission components could be separated.

**Acknowledgment.** We acknowledge support from the SNF, the Volkswagen Foundation, the RTN Network FUNMOLS, and the DFG. Furthermore, F.P. acknowledges funding of a Young Investigator Group, and F.E. thanks Christian Martin for useful communication.

**Supporting Information Available.** Details on experimental and theoretical procedures. This material is available free of charge via the Internet at <http://pubs.acs.org>.

## REFERENCES AND NOTES

- Nitzan, A.; Ratner, M. A. *Science* **2003**, *300* (5624), 1384–1389.
- Tao, N. J. *Nat. Nanotechnol.* **2006**, *1* (3), 173–181.
- Reed, M. A.; Zhou, C.; Muller, C. J.; Burgin, T. P.; Tour, J. M. *Science* **1997**, *278* (5336), 252–254.
- Reichert, J.; Ochs, R.; Beckmann, D.; Weber, H. B.; Mayor, M.; von Lohneysen, H. *Phys. Rev. Lett.* **2002**, *88* (17), 176804.
- Gonzalez, M. T.; Wu, S. M.; Huber, R.; van der Molen, S. J.; Schönenberger, C.; Calame, M. *Nano Lett.* **2006**, *6* (10), 2238–2242.
- Kiguchi, M.; Tal, O.; Wohlthath, S.; Pauly, F.; Krieger, M.; Djukic, D.; Cuevas, J. C.; van Ruitenbeek, J. M. *Phys. Rev. Lett.* **2008**, *101* (4), No. 046801.
- Park, J.; Pasupathy, A. N.; Goldsmith, J. I.; Chang, C.; Yaish, Y.; Petta, J. R.; Rinkoski, M.; Sethna, J. P.; Abruna, H. D.; McEuen, P. L.; Ralph, D. C. *Nature* **2002**, *417* (6890), 722–725.
- Van der Zant, H. S. J.; Osorio, E. A.; Poot, M.; O’Neill, K. *Phys. Status Solidi B* **2006**, *243* (13), 3408–3412.
- Chen, J.; Reed, M. A.; Rawlett, A. M.; Tour, J. M. *Science* **1999**, *286* (5444), 1550–1552.
- Seferos, D. S.; Trammell, S. A.; Bazan, G. C.; Kushmerick, J. G. *Proc. Natl. Acad. Sci. U.S.A.* **2005**, *102* (25), 8821–8825.
- Holmlin, R. E.; Ismagilov, R. F.; Haag, R.; Mujica, V.; Ratner, M. A.; Rampi, M. A.; Whitesides, G. M. *Angew. Chem., Int. Ed.* **2001**, *40* (12), 2316–2320.
- Yazdani, A.; Eigler, D. M.; Lang, N. D. *Science* **1996**, *272* (5270), 1921–1924.
- Dorogi, M.; Gomez, J.; Osifchin, R.; Andres, R. P.; Reifenberger, R. *Phys. Rev. B* **1995**, *52* (12), 9071–9077.
- Xu, B. Q.; Tao, N. J. *Science* **2003**, *301* (5637), 1221–1225.
- Haiss, W.; van Zalinge, H.; Higgins, S. J.; Bethell, D.; Hobenreich, H.; Schiffrin, D. J.; Nichols, R. J. *J. Am. Chem. Soc.* **2003**, *125* (50), 15294–15295.
- Venkataraman, L.; Klare, J. E.; Nuckolls, C.; Hybertsen, M. S.; Steigerwald, M. L. *Nature* **2006**, *442* (7105), 904–907.
- Li, C.; Pobelov, I.; Wandlowski, T.; Bagrets, A.; Arnold, A.; Evers, F. *J. Am. Chem. Soc.* **2008**, *130* (1), 318–326.
- Temirov, R.; Lassise, A.; Anders, F. B.; Tautz, F. S. *Nanotechnology* **2008**, *19* (6), No. 065401.
- Cui, X. D.; Primak, A.; Zarate, X.; Tomfohr, J.; Sankey, O. F.; Moore, A. L.; Moore, T. A.; Gust, D.; Harris, G.; Lindsay, S. M. *Science* **2001**, *294* (5542), 571–574.
- Wold, D. J.; Haag, R.; Rampi, M. A.; Frisbie, C. D. *J. Phys. Chem. B* **2002**, *106* (11), 2813–2816.
- Pecchia, A.; Di Carlo, A. *Rep. Prog. Phys.* **2004**, *67* (8), 1497–1561.
- Hybertsen, M. S.; Venkataraman, L.; Klare, J. E.; Cwhalley, A.; Steigerwald, M. L.; Nuckolls, C. *J. Phys.: Condens. Matter* **2008**, *20* (37), 374115.
- Haiss, W.; Nichols, R. J.; van Zalinge, H.; Higgins, S. J.; Bethell, D.; Schiffrin, D. J. *Phys. Chem. Chem. Phys.* **2004**, *6* (17), 4330–4337.
- Venkataraman, L.; Klare, J. E.; Tam, I. W.; Nuckolls, C.; Hybertsen, M. S.; Steigerwald, M. L. *Nano Lett.* **2006**, *6* (3), 458–462.
- Chen, F.; Li, X. L.; Hihath, J.; Huang, Z. F.; Tao, N. J. *J. Am. Chem. Soc.* **2006**, *128* (49), 15874–15881.
- Venkataraman, L.; Park, Y. S.; Whalley, A. C.; Nuckolls, C.; Hybertsen, M. S.; Steigerwald, M. L. *Nano Lett.* **2007**, *7* (2), 502–506.
- Leary, E.; Higgins, S. J.; van Zalinge, H.; Haiss, W.; Nichols, R. J.; Nygaard, S.; Jeppesen, J. O.; Ulstrup, J. J. *J. Am. Chem. Soc.* **2008**, *130* (37), 12204–12205.
- Haiss, W.; Wang, C. S.; Jitichati, R.; Grace, I.; Martin, S.; Batsanov, A. S.; Higgins, S. J.; Bryce, M. R.; Lambert, C. J.; Jensen, P. S.; Nichols, R. J. *J. Phys.: Condens. Matter* **2008**, *20* (37), 374119.
- Pauly, F.; Viljas, J. K.; Cuevas, J. C.; Schön, G. *Phys. Rev. B* **2008**, *77* (15), 155312.
- Benniston, A. C.; Harriman, A.; Li, P.; Patel, P. V.; Sams, C. A. *Chem.—Eur. J.* **2008**, *14* (6), 1710–1717.
- Smalley, J. F.; Sachs, S. B.; Chidsey, C. E. D.; Dudek, S. P.; Sikes, H. D.; Creager, S. E.; Yu, C. J.; Feldberg, S. W.; Newton, M. D. *J. Am. Chem. Soc.* **2004**, *126* (44), 14620–14630.
- Hou, S. M.; Zhang, J. X.; Li, R.; Ning, J.; Han, R. S.; Shen, Z. Y.; Zhao, X. Y.; Xue, Z. Q.; Wu, Q. *Nanotechnology* **2005**, *16* (2), 239–244.
- Bagrets, A.; Arnold, A.; Evers, F. *J. Am. Chem. Soc.* **2008**, *130* (28), 9013–9018.
- Lee, M. H.; Speyer, G.; Sankey, O. F. *J. Phys.: Condens. Matter* **2007**, *19* (21), 215204.
- Tomfohr, J.; Sankey, O. F. *J. Chem. Phys.* **2004**, *120* (3), 1542–1554.
- Finch, C. M.; Sirichantaropass, S.; Bailey, S. W.; Grace, I. M.; Garcia-Suarez, V. M.; Lambert, C. J. *J. Phys.: Condens. Matter* **2008**, *20* (2), No. 022205.
- Shaporenko, A.; Elbing, M.; Baszczyk, A.; von Hanisch, C.; Mayor, M.; Zharnikov, M. *J. Phys. Chem. B* **2006**, *110* (9), 4307–4317.
- (a) Vonlanthen, D.; Rotzler, J.; Neuburger, M.; Mayor, M. *Eur. J. Org. Chem.* **2010**, 120–125. (b) Vonlanthen, D.; Mishchenko, A.; Elbing, M.; Neuburger, M.; Wandlowski, T.; Mayor, M. *Angew. Chem., Int. Ed.* **2009**, *48* (47), 8886–8890.
- Meszaros, G.; Li, C.; Pobelov, I.; Wandlowski, T. *Nanotechnology* **2007**, *18*, 424004.
- Huang, Z. F.; Chen, F.; Bennett, P. A.; Tao, N. J. *J. Am. Chem. Soc.* **2007**, *129* (43), 13225–13231.
- Kamenetska, M.; Koentopp, M.; Whalley, A. C.; Park, Y. S.; Steigerwald, M. L.; Nuckolls, C.; Hybertsen, M. S.; Venkataraman, L. *Phys. Rev. Lett.* **2009**, *102* (12), 126805.
- Ulrich, J.; Esrail, D.; Pontius, W.; Venkataraman, L.; Millar, D.; Doerr, L. H. *J. Phys. Chem. B* **2006**, *110* (6), 2462–2466.
- Almenningen, A.; Bastiansen, O.; Fernholt, L.; Cyvin, B. N.; Cyvin, S. J.; Samdal, S. *J. Mol. Struct.* **1985**, *128* (1–3), 59–76.
- Dutt, G. B. *ChemPhysChem* **2005**, *6*, 413–418.
- Paulsson, M.; Brandbyge, M. *Phys. Rev. B* **2007**, *76* (11), 115117.
- Pauly, F.; Viljas, J. K.; Cuevas, J. C. *Phys. Rev. B* **2008**, *78* (3), No. 035315.
- Kondo, H.; Nara, J.; Kino, H.; Ohno, T. *J. Chem. Phys.* **2008**, *128* (6), No. 064701.
- Ahrlrichs, R.; Bär, M.; Häser, M.; Horn, H.; Kölmel, C. *Chem. Phys. Lett.* **1989**, *162* (3), 165–169.
- Eichkorn, K.; Treutler, O.; Öhm, H.; Häser, M.; Ahlrichs, R. *Chem. Phys. Lett.* **1995**, *242* (6), 652–660.
- Becke, A. D. *Phys. Rev. A* **1988**, *38* (6), 3098–3100.
- Perdew, J. P. *Phys. Rev. B* **1986**, *33* (12), 8822–8824.
- Eichkorn, K.; Weigend, F.; Treutler, O.; Ahlrichs, R. *Theor. Chem. Acc.* **1997**, *97* (1–4), 119–124.
- Weigend, F.; Häser, M.; Patzelt, H.; Ahlrichs, R. *Chem. Phys. Lett.* **1998**, *294* (1–3), 143–152.
- Arnold, A.; Weigend, F.; Evers, F. *J. Chem. Phys.* **2007**, *126* (17), 174101.

- (55) Pauly, F.; Viljas, J. K.; Huniar, U.; Häfner, M.; Wohlthat, S.; Bürkle, M.; Cuevas, J. C.; Schön, G. *New J. Phys.* **2008**, *10*, 125019.
- (56) Roper, M. G.; Skegg, M. P.; Fisher, C. J.; Lee, J. J.; Dhanak, V. R.; Woodruff, D. P.; Jones, R. G. *Chem. Phys. Lett.* **2004**, *389* (1–3), 87–91.
- (57) Bencini, A.; Rajaraman, G.; Totti, F.; Tusa, M. *Superlattices Microstruct.* **2008**, *46*, 4–9.
- (58) Evers, F.; Weigend, F.; Koentopp, M. *Phys. Rev. B* **2004**, *69* (23), 235411.
- (59) Reddy, P.; Jang, S. Y.; Segalman, R. A.; Majumdar, A. *Science* **2007**, *315* (5818), 1568–1571.
- (60) Quek, S. Y.; Venkataraman, L.; Choi, H. J.; Louie, S. G.; Hybertsen, M. S.; Neaton, J. B. *Nano Lett.* **2007**, *7* (11), 3477–3482.
- (61) Schmitteckert, P.; Evers, F. *Phys. Rev. Lett.* **2008**, *100* (8), No. 086401.
- (62) Haiss, W.; Martin, S.; Leary, E.; van Zalinge, H.; Higgins, S. J.; Bouffier, L.; Nichols, R. J. *J. Phys. Chem. C* **2009**, *113* (14), 5823–5835.
- (63) Xiao, X. Y.; Xu, B. Q.; Tao, N. J. *Nano Lett.* **2004**, *4* (2), 267–271.
- (64) Lörtscher, E.; Weber, H. B.; Riel, H. *Phys. Rev. Lett.* **2007**, *98* (17), 176807.